Space-Time Spectral Structure of a GLAS General Circulation Model and a Comparison with Observations

DAVID M. STRAUS[1] AND J. SHUKLA

Laboratory for Atmospheric Sciences, Modeling and Simulation Facility, NASA Goddard Space Flight Center, Greenbelt, MD 20771

(Manuscript received 18 August 1980, in final form 6 January 1981)

ABSTRACT

The wavenumber-frequency spectra of geopotential height have been computed from a winter simulation of a GLAS general circulation model, and are compared to the spectra obtained from 15 winters of observed analyses. The variances in several broadly defined space-time categories are presented, and their distribution with latitude and height discussed.

The low-frequency planetary waves (wavenumbers 1–4) in the model have substantially less variance than is observed and their latitudinal structure also differs from observations. The same is true for the medium-frequency planetary waves. The synoptic-scale waves (wavenumbers 5–10) with both low and medium frequencies are quite well reproduced by the model, with the total variances and their latitude-height structure comparing well to the observations. The net propagation tendency is examined for low-frequency planetary waves and the medium-frequency synoptic-scale waves. The model results show too much tendency for eastward propagation, the discrepancy being much larger in the case of the planetary waves. The model stationary waves were also examined. Their variance is considerably less than is observed, and their latitudinal structure incorrect. These findings are compared to the limited statistics available for the NCAR and GFDL models. The GLAS model's simulation of the synoptic-scale waves (with both low and medium frequencies) is apparently more realistic than that of the other models. The opposite is true for the stationary waves. All the models underpredict the low-frequency planetary-wave variance.

The differences between model and observed spectra are compared to (i) the range of interannual variability, and (ii) the estimated statistical uncertainties of the spectra. For the synoptic-scale waves the differences are generally smaller than either (i) or (ii), whereas for the planetary waves the differences are larger.

Possible causes for the GLAS model's underprediction of the stationary planetary wave variance are briefly discussed. It is suggested that the diabatic heating due to latent heat of condensation may play an important role. Further, evidence is presented indicating that the lack of variance in the model low-frequency planetary waves is closely related to the lack of variance in the stationary waves.

1. Introduction

The use of space-time spectral analysis in studying the general circulation of the atmosphere, both as observed and simulated, has shed new insights into the nature of large-scale atmospheric variability (Hayashi, 1971; Pratt and Wallace, 1976; Pratt, 1977; Hayashi and Golder, 1977; Fraedrich and Böttger, 1978; Schäfer, 1979; Pratt, 1979). The underlying concept is the expression of atmospheric data in terms of basis functions, each of which corresponds to a wave of a particular zonal wavenumber and frequency. To assure the completeness of this basis set, it is necessary to include both westward and eastward propagating waves. Attempts have been made to further distinguish standing waves (i.e., waves oscillating with fixed nodes) from propagating waves (Pratt, 1976; Hayashi, 1977), but Hayashi (1979) pointed out that it was more meaningful to use a spatially local framework in making this distinction. The basis set consisting of plane waves can be used to express the longitude and time variance of a field in terms of contributions from distinct wavenumbers and frequency bands, thus providing projections of atmospheric motions onto different space and time scales. Since the circulations implied by these projections are believed to owe their origin to at least somewhat distinct dynamical processes, space-time spectral analysis is useful in assessing the ability of a general circulation model (GCM) to simulate these processes. In particular, the stationary wave components are believed to be forced by orography and heating contrasts, while the presence of synoptic scale cyclone waves may be explained by baroclinic instability.

[1] Research completed while a Resident Research Associate under the auspices of the National Research Council, Washington, DC.

0022-4928/81/050902-16$08.00

The dynamical origins of the low-frequency planetary waves are not well understood and several hypotheses exist. Eliasen and Machenhauer (1965, 1969) have interpreted these waves as free atmospheric modes, while Charney and Straus (1980) have attributed them to the instability of the nonaxisymmetric stationary equilibria that exist in the presence of orography. Hirota (1971) has explained the existence of low-frequency stratospheric waves by the interaction of a fluctuating zonal-mean flow with stationary waves forced by orography. A potential source of kinetic energy for all transient planetary waves is the nonlinear interaction of smaller scales. The possibility of such a kinetic energy cascade from higher to lower wavenumbers was demonstrated for purely two-dimensional flow by Kraichnan (1967), while Charney (1971) discussed the relationship between two-dimensional flow and that of the atmosphere.

This paper presents space-time spectral analyses of a winter simulation by a Goddard Laboratory for Atmospheric Sciences general circulation model (GLAS GCM) and observed analyses for 15 winter seasons. The present study is limited to consideration of the geopotential height field north of 20°N. Emphasis is placed on the total variance and average propagation tendency in various broadly defined space and time categories, and on their distribution with latitude and height. The space and time scales studied include (i) stationary planetary waves (SPW's), which consist of the stationary component of zonal wavenumbers 1–4; (ii) stationary synoptic scale waves (SSW's), which consist of the stationary component of zonal wavenumbers 5–10; (iii) low-frequency planetary waves (LFPW's), consisting of wavenumbers 1–4 with periods of 7.5 to 90 days; (iv) low-frequency synoptic-scale waves (LFSW's), consisting of wavenumbers 5–10 with periods of 7.5 to 90 days; (v) medium-frequency planetary waves (MFPW's), consisting of wavenumbers 1–4 with periods of 2.8–6.9 days; and (vi) medium-frequency synoptic-scale waves (MFSW's), consisting of wavenumbers 5–10 with periods of 2.8–6.9 days. The transient wave categories (iii)–(vi) are defined to be exclusive of the annual cycle, which has been removed from the data before computing the variances on these scales. In addition to these wave categories, fluctuations of the zonally averaged geopotential also were computed, although the results are not discussed in detail in this paper.

Although an analysis of the general circulation strictly in the wavenumber and frequency domain is of intrinsic interest, the choice of the transient wave categories defined above also can be motivated by their loose association with more traditional meteorological entities. The synoptic-scale waves are associated with baroclinic systems such as cyclones. The propagation of these systems is reflected in the medium-frequency variance, while their life cycle of growth, maturity and decay contributes to the variance of the low-frequency category. Low-frequency planetary waves receive large contributions from blocking situations, whereas the medium-frequency planetary waves are known to be of importance in numerical weather prediction. Of course, these associations are only of a general nature and, in practice, there will be considerable overlap. Thus, for example, a particular blocking high might well contribute to categories (i), (ii) and (iv), as well as category (iii).

The main results of this paper relate to the comparison of the model spectra in these space-time categories with the observed winter spectra, averaged over the 15 winters. The model's stationary variance in both planetary- and synoptic-scale waves is considerably weaker than is observed, as is the case for the model's transient planetary waves, for both low and medium frequencies. In contrast, the model variance in the transient synoptic-scale wave categories (low and medium frequencies) compares quite well with observations. In all cases, the vertical structure of the model variances is comparable to that of the atmosphere, although some discrepancies exist. The horizontal structure of the model variances is in accord with the observations only for the transient synoptic-scale waves, while for both stationary and planetary-wave categories serious differences exist.

The propagation tendency is a measure of the relative strengths of the eastward and westward propagating motions. It has been calculated for the model, and has been compared to that of the atmosphere for the LFPW's and the MFSW's. The latter waves show almost exclusively eastward propagation in the model, as they do in the atmosphere. The model's LFPW's, however, show too much eastward propagation in the midlatitude upper troposphere. Section 2 contains descriptions of the GCM data, the observed data and the analysis technique. The results are presented and discussed in Section 3, and the conclusions are in Section 4.

2. Data and analysis

The GLAS GCM studied in this paper is based on the primitive equations in sigma coordinates. The domain is global, and extends from the surface to 10 mb in nine levels equally spaced in sigma. The horizontal resolution is 4° (latitude) × 5° (longitude), and the horizontal finite-differencing scheme used conserves kinetic energy and mean-square vorticity in the limit of nondivergent mass flux. Physical processes that are modeled include solar and terrestrial radiation, moist convection and turbulent subgrid-scale processes. The soil moisture is a prognostic variable, while both the sea surface tempera-

ture and surface albedo are prescribed. It is worth noting that a smooth, prescribed seasonal change in the sea surface temperature has been included. The model is further described in the work of Halem *et al.* (1979). The winter simulation that was studied was initialized with data valid for 1 January 1975, and was carried out for 90 days. The geopotential heights were interpolated from the model sigma levels to five levels of constant pressure (200, 300, 500, 700, and 850 mb) twice per day (0000 and 1200 GMT).

The stationary component of the height field was obtained as the time mean, and the variance in the various zonal wavenumbers calculated. In order to study the transient components, the GCM's annual cycle was estimated and removed from the data. This procedure is necessary to avoid the phenomenon of leakage (Bingham *et al.*, 1967), by which a large amount of power at frequencies too low to be resolved by the data (in this case the annual frequency) will cause spurious power to appear at *all* the frequencies that *are* resolved. The annual cycle was estimated by fitting a parabola to the time series at each grid point, and this estimate was subtracted from the data. The remaining time series was (at each grid point) then tapered with a cosine bell which affected the first and last 10% of the series (Bingham *et al.*, 1967). This limits the leakage from any components of the annual cycle *not* removed by the parabola to the low-frequency portion of the resolved spectrum. The tapering also reduces the total variance of the series, but since the observed data to which the model results are compared are tapered in exactly the same manner, this is considered not be a serious drawback. One desirable effect of the tapering is to sharply reduce the influence of the first week or so of the simulation on the spectra, a period during which model adjustment to the initial data was presumably taking place.

The observed data consisted of the National Meterological Center (NMC) objective analyses of upper air data for the years 1963–77 which were obtained by the Modeling and Simulation Facility from Mr. Roy Jenne at the National Center for Atmospheric Research. The 15 winter seasons were considered to start at 0000 GMT 1 January and to end at 1200 GMT 31 March (1200 GMT 30 March for 1964, 1968, 1972 and 1976). Each winter season was analyzed in exactly the same manner as the GCM simulation, and the average variances were obtained by taking the mean in each variance category across the 15 seasons.

The formulas giving the stationary and transient variances as functions of wavenumber and discrete frequency are derived in the Appendix. The transient variances correspond to the space-time deviations defined by Pratt (1979), with the understanding that the annual cycle has already been removed. The actual spectra were computed using the fast Fourier transform technique (Bingham *et al.*, 1967), and were summed over the frequency and wavenumber ranges described in the Introduction and defined more carefully in Table 1.

The degree of statistical confidence of the variances reported in each transient space-time category can be measured by the number of degrees of freedom ν, and these are given for each category in Table 2. The applicability of this measure of statistical uncertainty to the variances reported here depends on the assumptions that (i) the variable measured (in this case geopotential height) is distributed normally (in time), or the time series considered are of sufficient length, and (ii) the spectral density

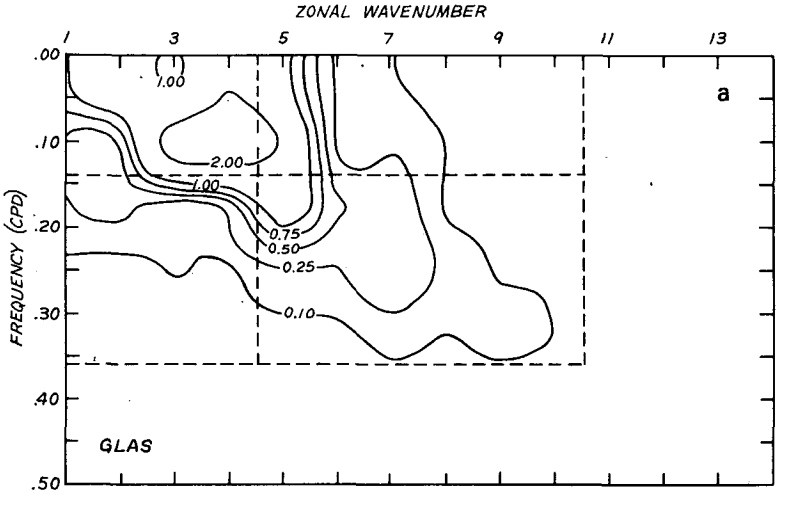

FIG. 1a. Wavenumber-frequency spectrum of the 500 mb geopotential height at 50°N in the GLAS GCM. Selected contours of the spectral density are shown, in units of 10^3 m^2 cpd^{-1}.

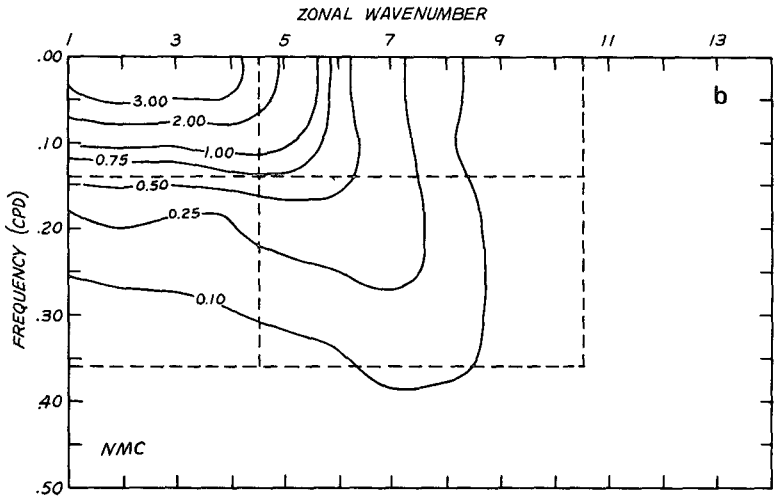

FIG. 1b. Wavenumber-frequency spectrum of the 500 mb geopotential height at 50°N from the NMC observations. Selected contours of the spectral density are shown, in units of 10^3 m^2 cpd^{-1}.

changes slowly over the wave number and frequency range considered. The results to be presented in Section 3 indicate that assumption (ii) is not very well satisfied. An alternate measure of uncertainty, namely the observed range of interannual variability, is considered in Section 3.

3. Results

a. GCM versus averaged observations

The wavenumber-frequency spectrum of the model 500 mb height field at 50°N is shown in Fig. 1a, and that for the observations in Fig. 1b. For a fixed wavenumber, the spectral density was obtained by summing the variances in a number of contiguous harmonic frequencies, and dividing this sum by the appropriate frequency range. This yielded a smoothed spectrum with a bandwidth of ~0.07 cpd (cycle per day).[2] The ratio of the GCM to the observed smoothed spectral density (GLAS/NMC) is reported in Fig. 1c. The boundaries of the four transient categories defined in Table 1 are indicated in the figures by the dashed lines. The space-time variances can be obtained by integrating the spectral density within the four boxes.

Significant features apparent in both the model and observed spectra are the concentration of spectral density in the low-frequency planetary

[2] The appearance of a nonzero spectral density at zero frequency is an artifact introduced for the sake of the visual clarity of the plots.

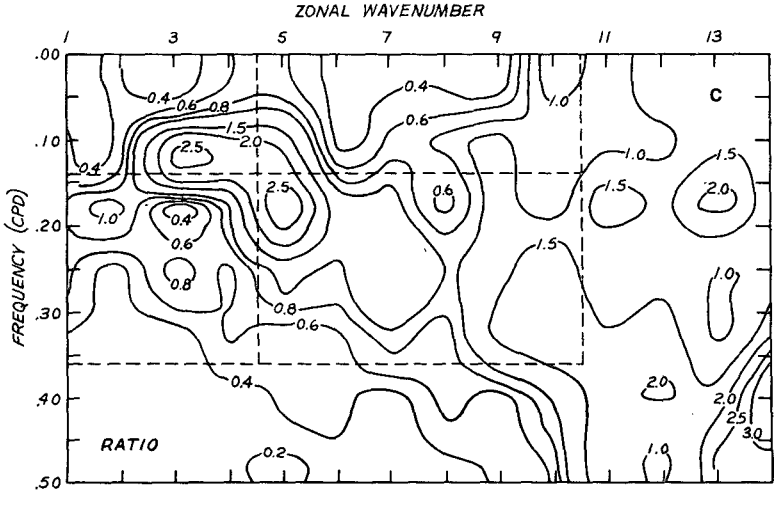

FIG. 1c. The ratio of model to observed spectral density.

TABLE 1. Description of space-time categories in terms of wavenumber and frequency ranges.

Space-time category	Range of wavenumbers	Range of frequency index m	Range of frequencies (cpd)*	Range of periods (days)
Stationary planetary waves	1–4	—	—	—
Stationary synoptic-scale waves	5–10	—	—	—
Low-frequency planetary waves	1–4	1–12	0.0111–0.1333	90–7.5
Low-frequency synoptic-scale waves	5–10	1–12	0.0111–0.1333	90–7.5
Medium-frequency planetary waves	1–4	13–32	0.1444–0.3556	6.9–2.8
Medium-frequency synoptic-scale waves	5–10	13–32	0.1444–0.3556	6.9–2.8

* The dimensional frequency f_m is related to m by $f_m = m/T$, $T = 90$ days.

waves, and the ridge of high density extending from the low frequencies and small wavenumbers to higher frequencies and wavenumbers. (These features have been noted by Pratt, 1979.) The model spectrum shows a distinct maximum at wavenumbers 3–5 with periods in the 8–15 day range, whereas the observed spectral density shows no such maximum but rather a continuous increase as the frequency and wavenumber decrease. The plot of the ratio of spectral densities (Fig. 1c) shows that the model spectrum is unrealistically large over a bandlike domain running from wavenumber 3 and a frequency of ~0.10 cpd to wavenumber 5 and a frequency of ~0.20 cpd. Elsewhere

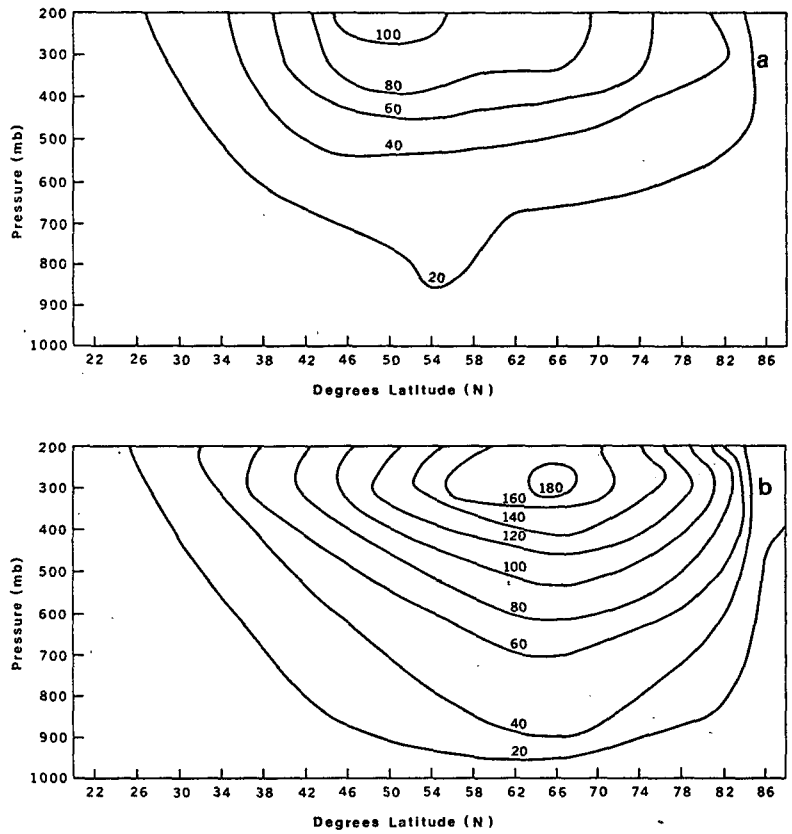

FIG. 2. The variance of the geopotential height in the low frequency planetary waves for the GLAS GCM (a), and for the 15-season average of winter observations (b). The units are 100 m². In Figs. 2–9, the data were available at five pressure levels (200, 300, 500, 700, 850 mb), and at every 4° of latitude from 22 to 86°N. For purpose of presenting the contours, the variance in Figs. 2–7 were assumed to vanish at 1000 mb.

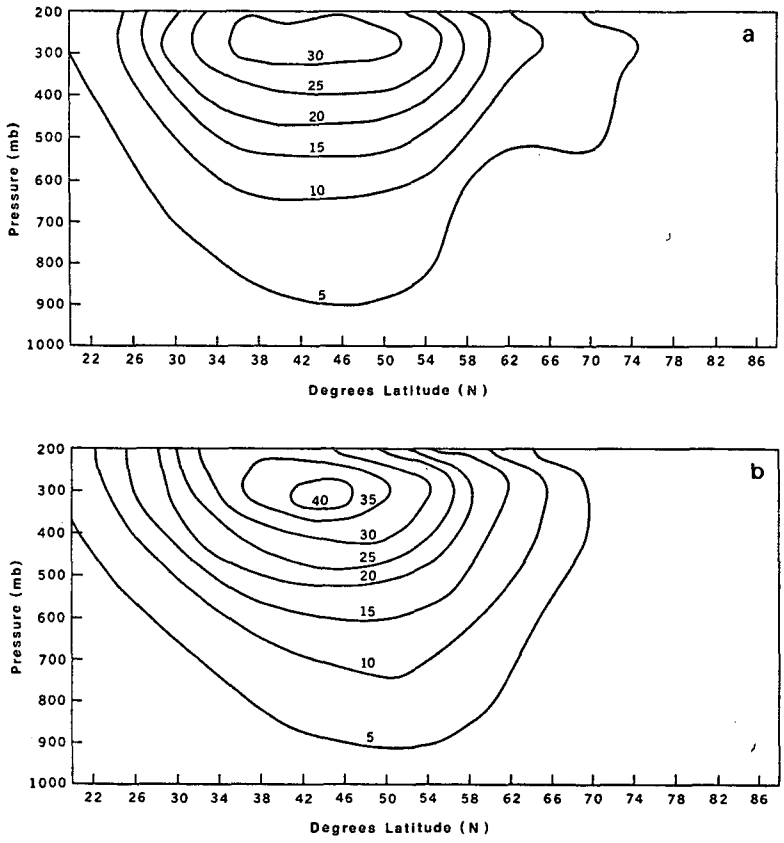

FIG. 3. The variance of the geopotential height in the low-frequency synoptic scale waves for the GLAS GCM (a), and for the 15-season average of winter observations (b). Units are 100 m^2.

within the four designated domains, the model spectrum is too weak. It is clear for at least the medium-frequency synoptic scales that the model shows enough variability, since the relative area enclosed by values of the ratio < 0.80 is small.

The vertical and meridional structure of the GCM and (averaged) observational variances in the four transient space-time categories are depicted in Figs. 2–5. The LFPW's in the GCM are much weaker than what is observed (Figs. 2a and 2b) and, moreover, their meridional structure is incorrect. The model LFPW's reach their maximum intensity at ~50°N, whereas the corresponding latitude for the observed LFPW's is 66°N. The vertical structure of the GCM LFPW's is generally in accord with observations, showing a monotonic increase in strength with height, although the decrease with height apparent in the observations above 300 mb is absent in the GCM results.

An examination of the LFSW's (Figs. 3a and 3b), on the other hand, shows that there is fairly good agreement between the GCM and the observations. The GCM's LFSW's are only slightly weaker than is observed, and the difference will turn out to be within the range of uncertainty associated with the spectra. (see Section 3b). Further, both the vertical and meridional dependence of the LFSW variance has been simulated correctly by the GCM.

The ability of the model to reproduce the observed MFPW variance is very limited, as is shown in Figs. 4a and 4b. Not only is the strength of the MFPW's in the model significantly less than that shown by observations, the meridional structure is poorly represented. Whereas the observed MFPW's reach a well-defined maximum at 70°N, the simulated variance shows a diffuse maximum stretching from 46 to 66°N. The vertical structure, however, is fairly well simulated by the GCM, with the variance increasing with height up to 300 mb.

The variance in the last transient wave category (MFSW's) is depicted in Figs. 5a and 5b, from which it is clear that the GCM is very successful in simulating these scales. The magnitude of the GCM's variance agrees well with observations, as does the vertical and meridional structure. A small discrepancy is present, however, in the meridional

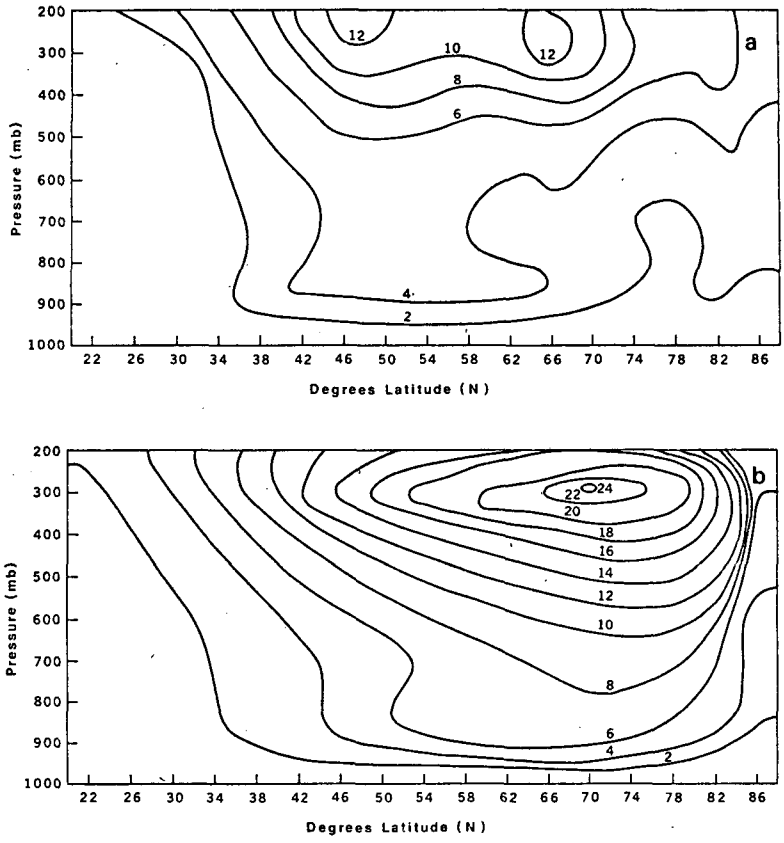

FIG. 4. The variance of the geopotential height in the medium-frequency planetary waves for the GLAS GCM (a), and for the 15-season average of winter observations (b). Units are 100 m^2.

structure, with the MFSW's of the GCM reaching their maximum intensity ~6° north of the observed.

In summary, the spatial scale of the transient disturbances seems to be the key element in determining the success of the GLAS GCM in reproducing observed atmospheric behavior. The planetary waves are not reproduced well for both long and medium time scales, while the synoptic-scale waves are well simulated for both time scales. It is of interest to compare the performance of the GLAS GCM with that of other GCM's in current use. Pratt (1979) compares space-time spectral analyses of the GCM's of the Geophysical Fluid Dynamics Laboratory (GFDL) and the National Center for Atmospheric Research (NCAR) with an analysis of four winters of observations. For the 500 mb geopotential height field at both 35 and 50°N, the LFPW's and MFSW's of both models are too weak (Pratt's Tables 1 and 2), although the discrepancies are generally less for the latter category. An examination of Figs. 3 and 5 of Pratt further suggests that the 500 mb LFSW's and MFPW's are also too weak in both models, at least at 35 and 50°N. Thus the problem of underpredicting the planetary wave variance seems to be common to all three models, while the GLAS model's success in simulating the strength of the baroclinic-scale waves is apparently not shared by the GFDL and NCAR models. These conclusions must be considered as tentative, however, until the space-time spectral analyses of the NCAR and GFDL models, (performed by Pratt predominantly for 500 mb at 35 and 50°N), are extended to more latitudes and levels.[3]

The variance in the stationary planetary waves and stationary synoptic scale waves of the GCM are compared to the averaged observations in Figs. 6a and 6b and 7a and 7b, respectively. The observed SPW variance (Fig. 6b) agrees quite well with the total stationary eddy variance presented by Lau (1979, his Fig. 4a), indicating that the planetary waves dominate the total stationary eddy

[3] In addition, the comparison between Pratt's work and this study is somewhat complicated by the fact that the observational data base is not identical (Pratt's observations span only four winters), nor are the definitions of the winter season.

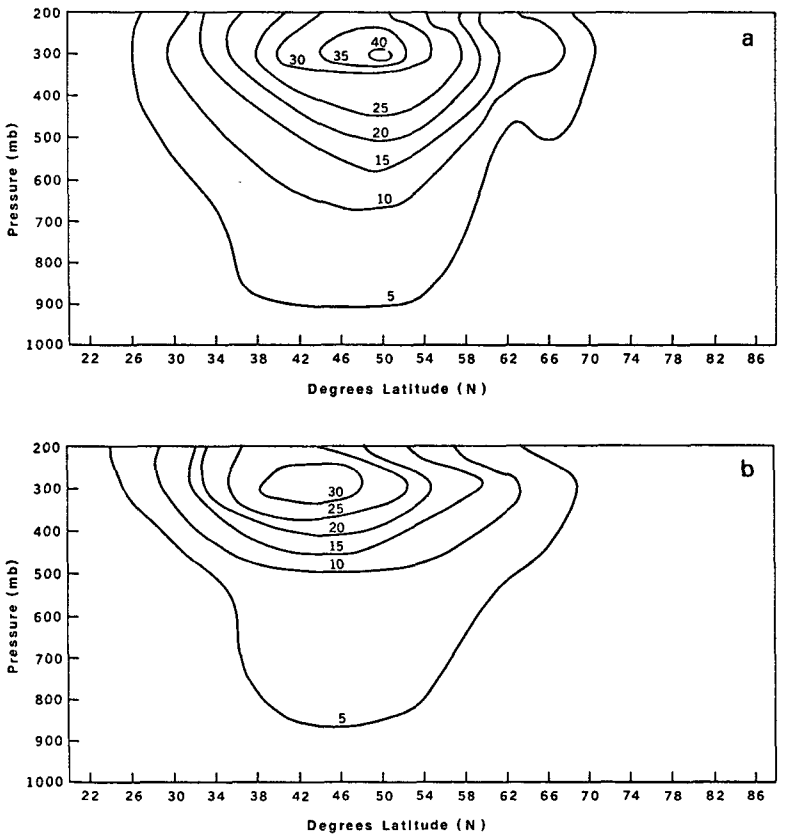

FIG. 5. The variance of the geopotential height in the medium-frequency synoptic scale waves for the GLAS GCM (a), and for the 15-season average of winter observations (b). Units are 100 m^2.

variance. The simulated SPW variance is very weak compared to observations. For example, the maximum GCM variance at 500 mb is only ~30% of the observed maximum. In addition, the meridional structure is quite different. The single maximum at 50°N in the averaged observations is replaced by two distinct maxima of equal strength at 50° and 70°N in the GCM. The vertical structure of the SPW variance in the GCM results is similar to the observed in that they both increase with height up to 300 mb; however, the observed decrease from 300 to 200 mb does not occur in the GCM.

An examination of the SSW variances (Figs. 7a and 7b) shows that, as expected, they are much smaller than the SPW variances. Again, the GCM does not reproduce the observed results; the variances are too weak and the maximum in the model variances occurs between 34 and 38°N, some 8° further south than in the observations. The vertical structure is again only roughly correct.

Pratt's study shows that the variance in the stationary geopotential height generated by both the NCAR and GFDL models compares well with the observations at 500 mb, at 35 and 50°N. Thus, in contrast to the situation with regard to the synoptic scale waves, the GLAS model does not share the apparent success of the NCAR and GFDL models in reproducing the SPW variance.

In order to study the propagation of waves in the various space-time categories, it is useful to introduce the net propagation tendency (NPT). This quantity measures the statistical tendency of the motions of a particular space and time scale to propagate zonally westward or eastward. A value of the NPT of +1.0 (−1.0) indicates pure westward (eastward) propagation. Fig. 8a shows the NPT of the GLAS GCM, averaged over the space and time scales corresponding to the LFPW's. The observed LFPW net propagation tendency, averaged over the 15 winters, is shown in Fig. 8b. In the interpretation of these results, it is important to recognize that the NPT is a statistical measure. Thus, for instance, knowing that the NPT is zero does not allow one to distinguish between standing waves (i.e., waves oscillating in place) and traveling waves which travel westward for only a portion of the ob-

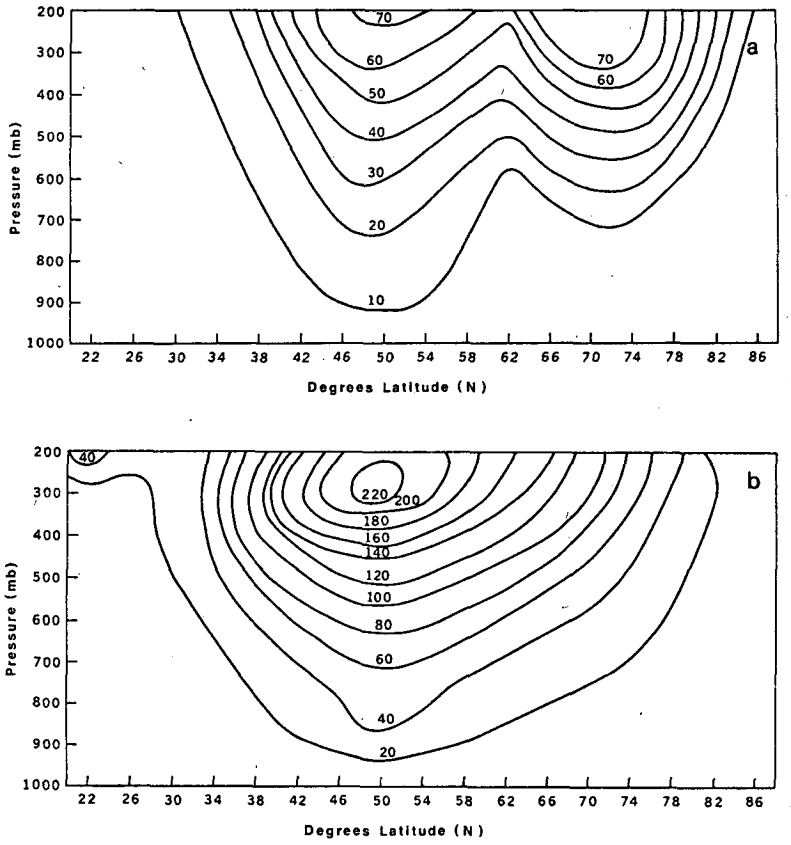

FIG. 6. The variance of the geopotential height in the stationary planetary waves for the GLAS GCM (a), and for the 15-season average of winter observations (b). Units are 100 m^2.

served period, but travel eastward for the remaining time. Thus, the generally small values of the NPT in Fig. 8b indicate that the LFPW's observed in nature have no strong preference for propagating westward as opposed to eastward, or vice versa; the relative strengths of the propagating versus standing components cannot be assessed. Comparison of Figs. 8a and 8b indicates that the propagation characteristics of the model's LFPW's are not in accord with those of nature. In the lower troposphere, the GCM results are almost completely out of phase with the observations, since they show eastward propagation at midlatitudes and westward propagation at high latitudes. In the upper troposphere south of 50°N, both the GCM and the observed LFPW's show a tendency toward eastward propagation; but this tendency is far too strong in the GCM. Overall, the major deficiency in the model LFPW's appears to be an unrealistically strong eastward propagation tendency in midlatitudes. It must be noted, however, that due to the interannual variability of the NPT, the process of taking the 15-season mean results in some degree of cancellation. Even so, the large negative values of the NPT in Fig. 8a are unrealistic.

The NPT of the MFSW's is shown in Fig. 9a for the GCM and Fig. 9b for the observations. The observed MFSW's show a tendency toward eastward propagation almost everywhere, with this tendency reaching a maximum (corresponding to almost pure eastward propagation) in the midlatitude upper troposphere. The model reproduces this behavior fairly well, the only discrepancy being that the net eastward propagation tendency is somewhat too strong. Thus the GLAS GCM simulates the baroclinic-scale waves rather well, reproducing not only their amplitude but also their propagation characteristics as well.

The time-variability of the zonally averaged geopotential height can be studied by examining the total variance in the low-frequency and medium-frequency portions of the spectrum. Such a study was carried out, although the results are not reported in detail. This variance is generally an order of magnitude less than that of the LFPW's. With regard to model performance, it was found that the GCM

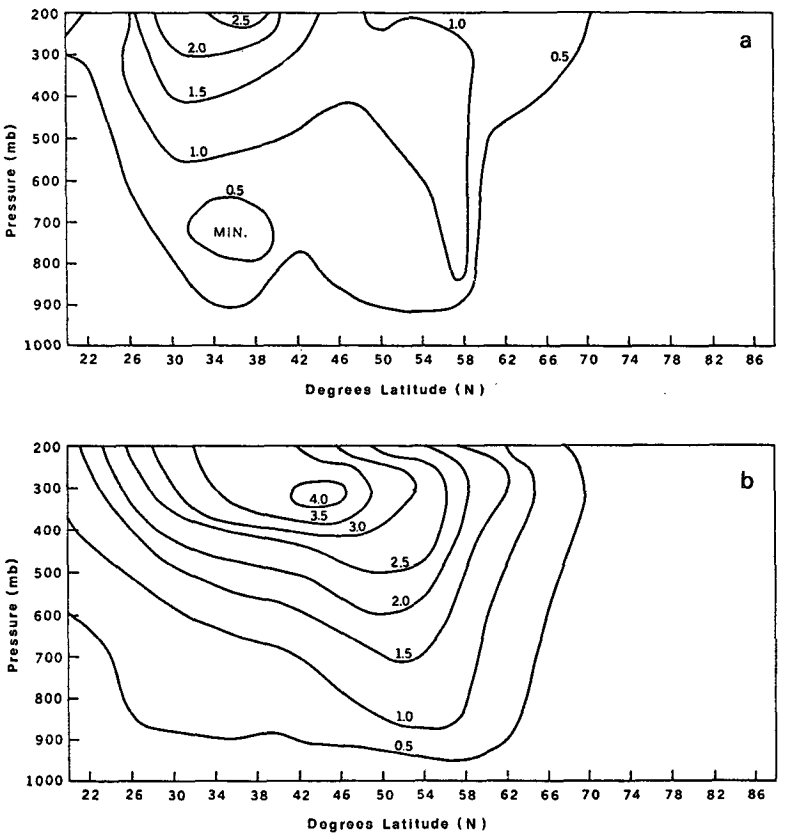

FIG. 7. The variance of the geopotential height in the stationary synoptic-scale waves for the GLAS GCM (a), and for the 15-season average of winter observations (b). Units are 100 m^2.

underestimates the variability of the zonally averaged height field, the discrepancy being greater for low frequencies than it is for medium frequencies.

b. Interannual variability and statistical uncertainty

Since the atmosphere exhibits a certain amount of interannual variability, a description of observed winter spectra should include not only their mean values but also a measure of their variability. Similar comments apply to the model spectra, since different model simulations of the winter season will in general not be identical. Thus the comparison made in this paper between the model spectra (one realization only) and the observed spectra (average over 15 realizations) is not complete without a discussion of the variability of *both* the model and observed spectra. The aim of such a discussion here is to establish whether differences found between the model and observational spectra are significant in light of their variability.[4]

One approach is to compare the model spectra (and their dependence on latitude and height) to each of the 15 individual observed spectra, to determine if the model spectra more closely resemble those of a particular winter than they do the average. Such a comparison has been made for the SPW's, which for the model were substantially weaker than the averaged observations, and also had a very different horizontal structure (Figs. 6a and 6b). The model SPW's continue to be much too weak when compared individually to those of each observed winter. However, the doubly-peaked horizontal structure of the model SPW's closely resembles the horizontal structure of the SPW's observed in 1963 (not shown). Whether or not this similarity is a coincidence remains to be investigated.

Another approach is to consider the range of interannual variability separately at each latitude and height. An example of this approach is given in Fig.

[4] The problem is further compounded by the fact that the boundary conditions (sea surface temperature, snow/ice cover, soil moisture, etc.) in nature fluctuate from year to year, whereas those used in the model integration were climatological averages. Thus, the model may not be able to reproduce some of the more extreme situtations that are observed simply because no account is taken of anomalous boundary conditions.

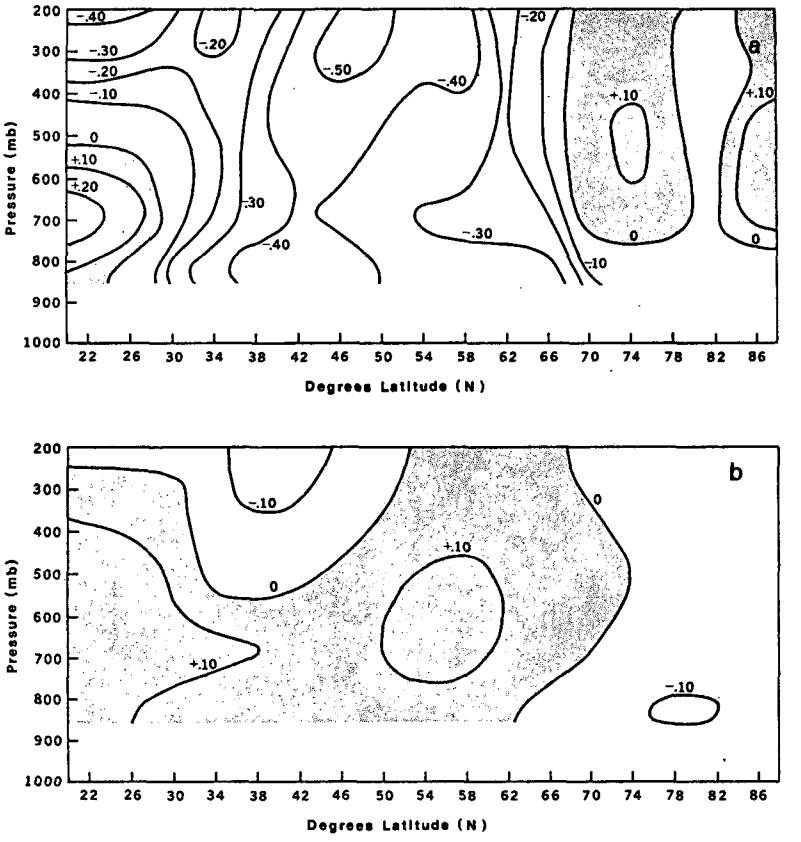

FIG. 8. The net propagation tendency of the geopotential height, averaged over the low-frequency planetary waves for the GLAS GCM (a), and for the 15-season average of winter observations (b). Regions of positive net propagation tendency are shaded.

10, which shows the LFPW variance at 500 mb for both the GLAS GCM (solid line) and the averaged observations (dashed line). The dotted lines represent, (at any given latitude), the maximum and minimum variance in the LFPW's over the 15 winters. The difference between the model and observed LFPW variance is significant in that, at most latitudes, the model variance is well outside the range of interannual variability.

The same comparisons are made for the LFSW's in Fig. 11 and for the MFSW's in Fig. 12. From Fig. 11 the conclusion is drawn that the differences between the variance in the simulated and observed LFSW's are not significant, as previously mentioned. For the MFSW's (Fig. 12), the model variance falls within the range of interannual variability, if allowance is made for the slight northward shift of this variance compared to observations.

Yet a third approach is a more traditional statistical one. This method proceeds from the assumption that atmospheric spectra follow chi-squared distributions, so that their uncertainty can be measured by the degrees of freedom listed in Table 2. Examples of such error estimates are given in Figs. 10–12, in which the 95% confidence limits are indicated by the vertical bars on both the model and observed spectra.[5] In each case, the observed spectrum has much less uncertainty associated with it than does the model spectrum because it represents a 15-season average and hence has many more degrees of freedom. Consideration of these estimates of uncertainty leads to the same conclusions that were reached in the preceding paragraph: The model's LFPW's are significantly weaker than observed, while the LFSW's and MFSW's are not significantly different than observations.

4. Conclusions

The space-time spectral analyses of the GLAS GCM and the observations indicate that the model

[5] Since the variances have been plotted on a linear scale and not a logarithmic scale, the error bars are not symmetric about the calculated variance. Further, the size of the error bars is not independent of the size of the calculated variance, the former being proportional to the latter.

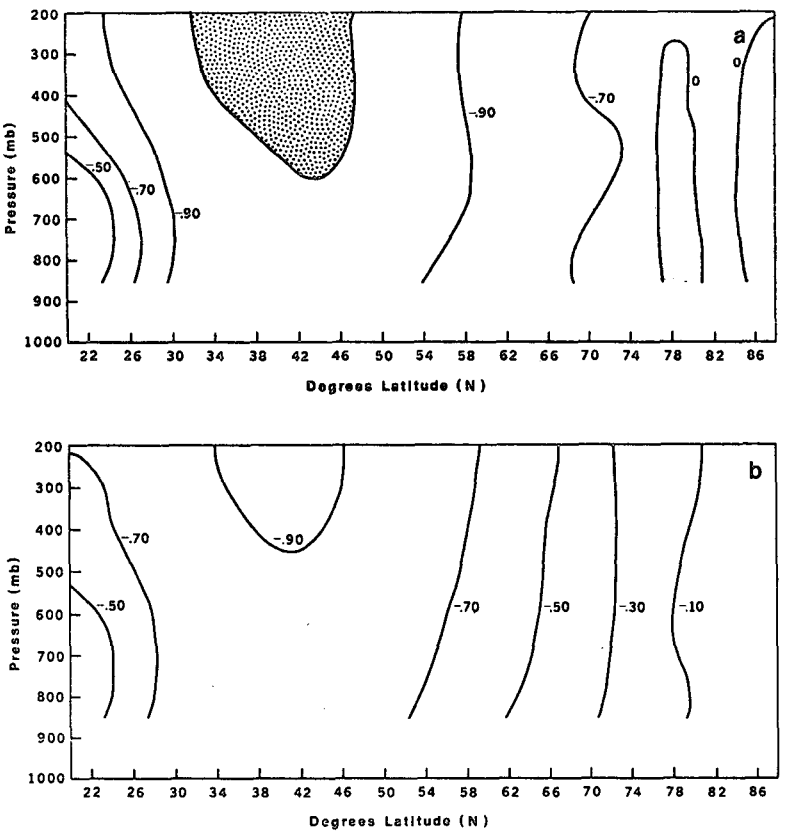

FIG. 9. The net propagation tendency of the geopotential height, averaged over the medium-frequency synoptic scale waves for the GLAS GCM (a), and for the 15-season average of winter observations (b). Regions of positive net propagation tendency are shaded. Stippling denotes a region for which the net propagation tendency is less than −0.98.

variance in both the stationary waves and the transient planetary waves is too weak, while the model variance in synoptic scales is comparable to the observations. A study of the propagation tendency of transient low frequency planetary waves and medium frequency synoptic scale waves indicates that the model predicts too much eastward propagation, the qualitative discrepancy being much larger for the former wave category. A comparison with the limited statistics available for the NCAR and GFDL models suggests that the GLAS model better reproduces the medium frequency synoptic-scale wave variance, but that the NCAR and GFDL models simulate the stationary planetary waves more successfully. It is noteworthy that all three models substantially underpredict the transient planetary wave variance.

The successful simulation of the synoptic scale waves by the GLAS GCM indicates that the horizontal and vertical resolution and the finite-differencing scheme used are adequate to resolve well the fundamental process of baroclinic instability.

The stationary waves in the real atmosphere owe their existence to the presence of the nonaxisymmetric forcings of topography and diabatic heating contrasts, including latent heat release (Charney and Eliassen, 1949; Smagorinsky, 1953). Thus it is natural to ascribe the GCM's lack of stationary wave variance to possible errors in the model formulation of these forcings. With regard to latent heat release, the GLAS GCM simulation of rainfall in the mid-latitude Northern Hemisphere shows overall agreement with the winter climatology of Schutz and Gates (1972).[6] However, in comparison with satellite-derived rainfall rates (Rao *et al.*, 1976), or with the simulated rainfall of the GFDL model (Manabe *et al.*, 1974), the GLAS model substantially underpredicts the rainfall in the subtropical western Pacific. Very recently, a new winter integration of the GLAS

[6] Schutz, C., and W. L. Gates, 1972: Supplemental global climatic data: January. A report prepared for the Advanced Research Project Agency R-915/1-ARPA (order No. 189-1) by Rand Corporation, Santa Monica, CA.

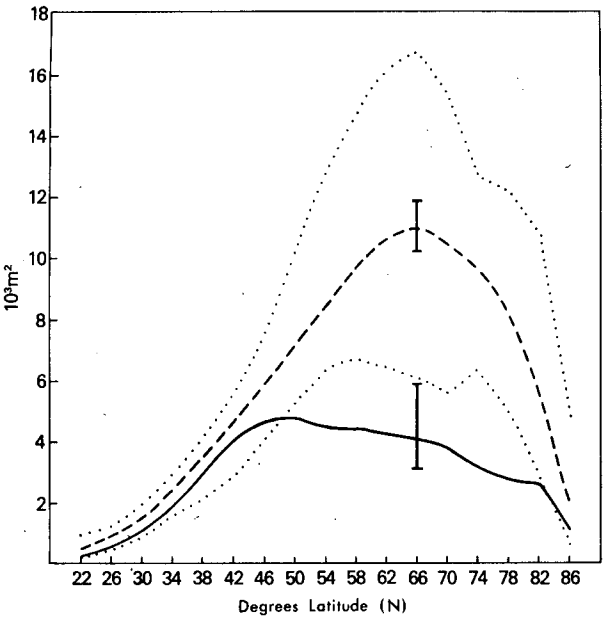

FIG. 10. The variance of the geopotential height at 500 mb for the low-frequency planetary waves for the GLAS GCM (solid line), and for the 15-season average of winter observations (dashed line). The error bars indicate the 95% confidence level. The dotted lines represent, at any given latitude, the maximum and minimum variance over the 15 winters.

model has been performed, in which several deficiencies in the boundary layer have been corrected. The main effect of these changes was to increase the precipitation over the oceans, and decrease it over land. The new model integration showed considerably more precipitation over both the tropical and subtropical oceans. A preliminary analysis of this new run indicates that the stationary planetary waves resemble the observations much more closely than do the SPW's of the integration that is discussed here. Research is currently underway to determine if the improvement in SPW variance is indeed due to the increase in precipitation.

There also may be deficiencies in the GLAS model representation of orographic effects, not only because the model orography has been artificially smoothed (Halem *et al.*, 1979), but also because the horizontal finite-differencing scheme cannot produce the correct dynamical response to high and steep mountains (Arakawa and Lamb, 1980).

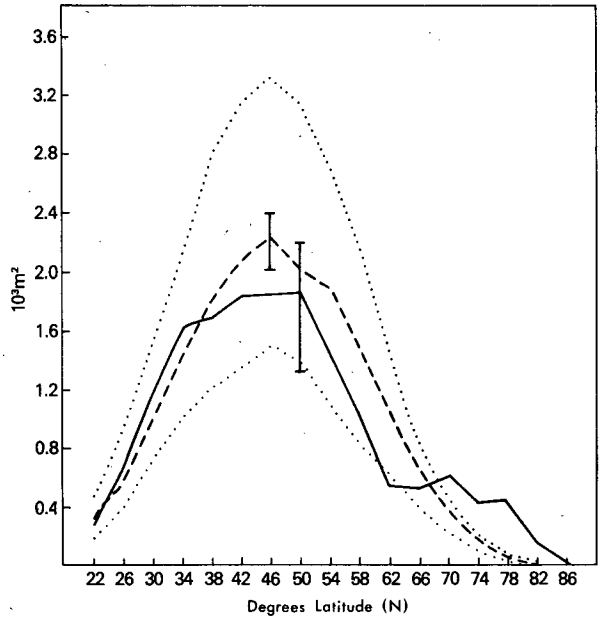

FIG. 11. The variance of the geopotential height at 500 mb for the low-frequency synoptic-scale waves, depicted exactly as in Fig. 10.

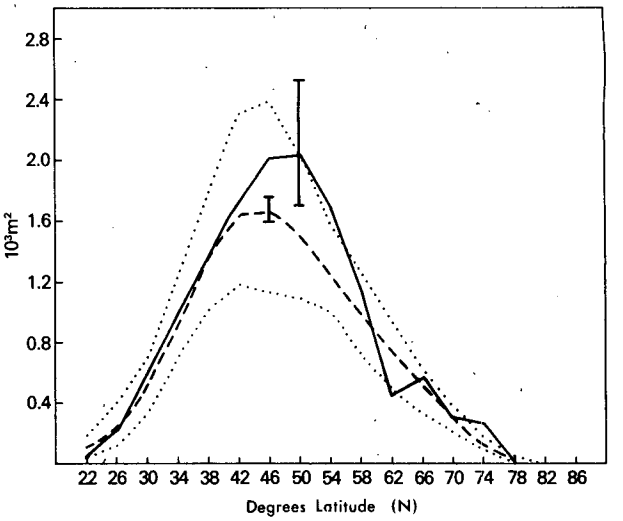

FIG. 12. The variance of the geopotential height at 500 mb for the medium-frequency synoptic-scale waves, depicted exactly as in Fig. 10.

TABLE 2. Degrees of freedom (ν) for each space-time category. The degrees of freedom for one season apply to either observed or simulated data. The general formula for ν is $\nu = 2N_kN_mN_sN_t$, where N_k is the number of wavenumbers summed over, N_m the number of frequency indices (harmonic frequencies) summed over, N_s the number of seasons averaged over, and $N_t = 0.87$ a correction factor to take into account the cosine-bell tapering (Julian, 1971).

Space-time category	Degrees of freedom for one season	Degrees of freedom for 15-season average
Low-frequency planetary waves	84	1260
Low-frequency synoptic-scale waves	125	1875
Medium-frequency planetary waves	139	2085
Medium-frequency synoptic-scale waves	209	3135

The low-frequency planetary waves in the GLAS GCM not only have too little variance, but they also exhibit more eastward propagation than is observed, south of 70°N. Pratt and Wallace (1976) have shown that the observed low-frequency planetary waves can often be represented as a sum of two modes. The first is westward moving and has an equivalent barotropic structure, while the second moves eastward and is more baroclinic. It appears that the first mode is absent in the model data.

A connection between the observed stationary and low-frequency planetary waves is suggested in the work of Kao and Lee (1977), who studied the winter kinetic energy budget in wavenumber-frequency space. They find that nonlinear interactions between stationary planetary waves and eastward moving LFPW's extract kinetic energy from these latter waves (at least at 40°N, 500 mb), whereas the interaction between the SPW's and the westward moving LFPW's tend to supply energy to the latter. This would imply that if the SPW-LFPW interactions were too weak (perhaps because the SPW's themselves are too weak), the energy of eastward moving LFPW's would be increased, and that of westward moving LFPW's decreased. That this mechanism is in fact operating in the GLAS GCM is confirmed by the work of Chen *et al.* (1980), who apply the Kao-Lee analysis scheme to the same GLAS model simulation studied in this paper. They find that the SPW-LFPW nonlinear interactions are much too weak in the model.

A more general explanation of the inability of the GLAS GCM to fully simulate the planetary waves may be the presence of an imposed rigid upper lid in the model atmosphere, a topic discussed by Lindzen *et al.* (1968). This explanation, of course, would apply equally well to the underprediction of planetary waves in other GCM's. Clearly, more research is needed to determine the causes of the model deficiencies discussed in this paper, and to ascertain whether or not the causes are model-dependent.

Acknowledgments. We would like to acknowledge our appreciation and thanks to Dr. R. W. Pratt, whose comments and advice at the planning stages of this work were very welcome, and to William Byerly, who was responsible for the programming in the early stages of the calculations. Thanks are also due to Karen DeHenzel for typing the manuscript, and to Laura Rumburg for drafting the figures. One of us (DMS) would like to acknowledge the support of the National Research Council.

APPENDIX

Space-Time Spectral Analysis

The purpose of this Appendix is to develop the formulas of space-time spectral analysis, following the ideas and notation of Hayashi (1971). Consider a function $X(j, r)$ of discrete time r and discrete longitude j. The ranges of r and j are

$$-n \leq r \leq n - 1,$$

$$-n_G \leq j \leq n_G - 1,$$

in which the total number of discrete times ($N = 2n$) and the total number of discrete points ($N_G = 2n_G$) are assumed even. If the time interval between discrete times is Δ (here equal to 0.5 day), then the continuous time variable (t) and space variable (λ) are given by

$$t_r = r\Delta,$$

$$\lambda_j = 2\pi j/N_G.$$

The variable t_r is abbreviated as t.

1. Stationary waves

The field $X(j, r)$ can be written as

$$X(j, r) = c_0(r) + \sum_{k=1}^{n_G} [c_k(r) \cos k\lambda_j + s_k(r) \sin k\lambda_j], \quad \text{(A1)}$$

where k is the dimensionless wavenumber, and[7]

$$c_k(r) = 2/N_G \sum_{j=-n_G}^{n_G-1} X(j, r) \cos(2\pi kj/N_G)$$

$$= 2/N_G \sum_{j=-n_G}^{n_G-1} X(j, r) \cos\lambda_j k, \quad \text{(A2a)}$$

and

$$s_k(r) = 2/N_G \sum_{j=-n_G}^{n_G-1} X(j, r) \sin\lambda_j k, \quad \text{(A2b)}$$

for $1 \leq k \leq n_G - 1$.

By taking the time average of Eq. (A1), a formula is obtained for the stationary field in terms of a zonal flow and stationary waves. Taking the longitudinal variance of this stationary field yields

$$1/N_G \sum_{j=-n_G}^{n_G-1} [\overline{X(j)}]^2 = (\overline{c_0})^2 + \tfrac{1}{2} \sum_{k=1}^{n_G} \left[(\overline{c_k})^2 + (\overline{s_k})^2\right]$$

$$\equiv \text{SZ} + \text{SW}, \quad \text{(A3)}$$

where an overbar denotes a time average, SZ denotes the contribution of the stationary zonal flow to the variance and SW that of the stationary waves.

2. Transient waves

We now assume that the time average and seasonal trend have been removed. An equation of the

[7] Throughout the Appendix, terms involving $k = n_G$ and $m = n$ should have certain factors of 2 not associated with the other values of k and m. For simplicity of presentation, and since these special values of k and m do not enter the numerical results presented, these factors are not given here.

form (A1) still holds, where

$$c_k(r) = c_{k,0} + \sum_{m=1}^{n} (A_{k,m} \cos 2\pi f_m t + B_{k,m} \sin 2\pi f_m t), \quad 0 \leq k \leq n_G, \tag{A4a}$$

$$s_k(r) = s_{k,0} + \sum_{m=1}^{n} (a_{k,m} \cos 2\pi f_m t + b_{k,m} \sin 2\pi f_m t), \quad 1 \leq k \leq n_G - 1. \tag{A4b}$$

Here

$$A_{k,m} = 2/N \sum_{r=-n}^{n-1} c_k(r) \cos 2\pi f_m t, \tag{A5a}$$

$$B_{k,m} = 2/N \sum_{r=-n}^{n-1} c_k(r) \sin 2\pi f_m t, \tag{A5b}$$

and similar formulas hold for $a_{k,m}$ and $b_{k,m}$ in terms of $s_k(r)$. In Eqs. (A4), (A5), the discrete (dimensionless) frequency m is related to the continuous (dimensional) frequency f_m by $f_m = m/N\Delta$. The stationary components $c_{k,0}$ and $s_{k,0}$ have been formally retained in (A4), although they vanish by assumption. Setting them equal to zero, the total space-time variance is

$$\begin{aligned}(\tilde{X}^2) &\equiv 1/N \sum_{r=-n}^{n-1} 1/N_G \sum_{j=-n_G}^{n_G-1} [X(j, r)]^2 \\ &= \tfrac{1}{2} \sum_{m=1}^{n} (A_{0,m}^2 + B_{0,m}^2) \\ &\quad + \tfrac{1}{4} \sum_{m=1}^{n} \sum_{k=1}^{n_G} (A_{k,m}^2 + B_{k,m}^2 + a_{k,m}^2 + b_{k,m}^2) \\ &\equiv \mathrm{TZ} + \mathrm{TW}. \end{aligned} \tag{A6}$$

The term TZ refers to the contribution of the transient zonal components to the total space-time variance, while TW refers to the contribution of the transient wave components.

In order to discuss zonal propagation, it is useful to write $X(j, r)$ as

$$\begin{aligned}X(j, r) &= \sum_{m=1}^{n} (A_{0,m} \cos 2\pi f_m t + B_{0,m} \sin 2\pi f_m t) \\ &\quad + \sum_{k=1}^{n_G} \sum_{m=1}^{n} [W_{k,m} \cos(k\lambda_j + 2\pi f_m t + \phi_{k,m}^W) \\ &\quad + E_{k,m} \cos(k\lambda_j - 2\pi f_m t + \phi_{k,m}^E)]. \end{aligned} \tag{A7}$$

The first term gives the fluctuations of the zonally averaged flow, whereas the second represents the transient waves projected onto a basis set consisting of westward traveling waves (with amplitude $W_{k,m}$, phase $\phi_{k,m}^W$) and eastward traveling waves (with amplitude $E_{k,m}$, phase $\phi_{k,m}^E$).

The quantities $A_{k,m}$, $B_{k,m}$, $a_{k,m}$ and $b_{k,m}$ of Eqs. (A4) can then be written as

$$\left.\begin{aligned} A_{k,m} &= W_{k,m} \cos\phi_{k,m}^W + E_{k,m} \cos\phi_{k,m}^E \\ B_{k,m} &= -W_{k,m} \sin\phi_{k,m}^W + E_{k,m} \sin\phi_{k,m}^E \\ a_{k,m} &= -W_{k,m} \sin\phi_{k,m}^W - E_{k,m} \sin\phi_{k,m}^E \\ b_{k,m} &= -W_{k,m} \cos\phi_{k,m}^W + E_{k,m} \cos\phi_{k,m}^E \end{aligned}\right\}, \tag{A8}$$

and the transient wave variance of Eq. (A6) as

$$\begin{aligned}\mathrm{TW} &= \tfrac{1}{2} \sum_{k=1}^{n_G} \sum_{m=1}^{n} (W_{k,m}^2 + E_{k,m}^2) \\ &\equiv \sum_{k=1}^{n_G} \sum_{m=1}^{n} (PW_{k,m} + PE_{k,m}). \end{aligned} \tag{A9}$$

Thus $PW_{k,m}$ and $PE_{k,m}$ give the contribution of the westward and eastward traveling waves, respectively, for wavenumber k and frequency m. The net propagation tendency (NPT) is then defined as

$$\mathrm{NPT}_{k,m} = (PW_{k,m} - PE_{k,m})/(PW_{k,m} + PE_{k,m}), \tag{A9a}$$

so that a value of $+1.0$ (-1.0) indicates pure westward (eastward) propagation.

To relate the space-time spectral analysis to conventional time series analyses of the series $c_k(r)$, $s_k(r)$, one must introduce the one-sided power spectra $P_m(c_k)$, $P_m(s_k)$, cospectrum $L_m(c_k, s_k)$ and quadrature spectrum $Q_m(c_k, s_k)$. It is straightforward to show that these quantities are given by

$$\left.\begin{aligned} P_m(c_k) &= \tfrac{1}{2}(A_{k,m}^2 + B_{k,m}^2) \\ P_m(s_k) &= \tfrac{1}{2}(a_{k,m}^2 + b_{k,m}^2) \\ L_m(c_k, s_k) &= \tfrac{1}{2}(A_{k,m}a_{k,m} + B_{k,m}b_{k,m}) \\ Q_m(c_k, s_k) &= \tfrac{1}{2}(B_{k,m}a_{k,m} - A_{k,m}b_{k,m}) \end{aligned}\right\}. \tag{A10}$$

Hence, $PW_{k,m}$ and $PE_{k,m}$ can be written as

$$\left.\begin{aligned} PW_{k,m} &= \tfrac{1}{4}[P_m(c_k) + P_m(s_k) + 2Q_m(c_k, s_k)] \\ PE_{k,m} &= \tfrac{1}{4}[P_m(c_k) + P_m(s_k) - 2Q_m(c_k, s_k)] \end{aligned}\right\}. \tag{A11}$$

The net propagation tendency is then

$$\mathrm{NPT}_{k,m} = Q_m(c_k, s_k)/(PW_{k,m} + PE_{k,m}). \tag{A12}$$

REFERENCES

Arakawa, A., and V. R. Lamb, 1981: A potential enstrophy and energy-conserving scheme for the shallow-water equations. *Mon. Wea. Rev.*, **109**, 18–36.

Bingham, C., M. D. Godfrey and J. W. Tukey, 1967: Modern techniques of power spectrum estimation. *IEEE Trans. Audio Electroacoustics*, **AU-15**, 56–66.

Charney, J. G., 1971: Geostrophic turbulence. *J. Atmos. Sci.*, **28**, 1087–1095.

——, and A. Eliassen, 1949: A numerical method for predicting the perturbations of the middle latitude westerlies. *Tellus*, **1**, 38–54.

——, and D. M. Straus, 1980: Form-drag instability, multiple

equilibria and propagating planetary waves in baroclinic, orographically forced planetary wave systems. *J. Atmos. Sci.*, **37**, 1157–1176.

Chen, T.-C., H. G. Marshall and J. Shukla, 1980: Spectral Analysis and Diagnosis of Nonlinear Interactions of large-scale moving waves at 200 mb of the GLAS general circulation model. *Mon. Wea. Rev.*, **109**, 959–974.

Eliasen, E., and B. Machenhauer, 1965: A study of the fluctuations of the atmospheric planetary flow patterns represented by spherical harmonics. *Tellus*, **17**, 220–238.

——, and B. Machenhauer, 1969: On the observed large-scale atmospheric wave motions. *Tellus*, **21**, 149–166.

Fraedrich, K., and H. Böttger, 1978: A wavenumber-frequency analysis of the 500 mb geopotential at 50°N. *J. Atmos. Sci.*, **35**, 745–750.

Halem, M., J. Shukla, Y. Mintz, M. L. Wu, R. Godbole, G. Herman and Y. Sud, 1979: Comparisons of observed seasonal climate features with a winter and summer numerical simulation produced with the GLAS general circulation model. Report of the JOC Study Conf. on Climate Models: Performance, Intercomparison and Sensitivity Studies, Vol. I, *GARP Publ. Series*, No. 22, 207–253. WMO, Geneva, Switzerland.

Hayashi, Y., 1971: A generalized method of resolving disturbances into progressive and retrogressive waves by space Fourier and time cross-spectral analysis. *J. Meteor. Soc. Japan.*, **49**, 125–178.

——, 1977: On the coherence between progressive and retrogressive waves and a partition of space-time power spectra into standing and traveling parts. *J. Appl. Meteor.*, **16**, 368–373.

——, 1979: A generalized method of resolving transient disturbances into standing and traveling waves by space-time spectral analysis. *J. Atmos. Sci.*, **36**, 1017–1029.

——, and D. G. Golder, 1977: Space-time spectral analysis of mid-latitude disturbances appearing in a GFDL general circulation model. *J. Atmos. Sci.*, **34**, 237–262.

Hirota, I., 1971: Excitation of planetary Rossby waves in the winter stratosphere by periodic forcing. *J. Meteor. Soc. Japan*, **49**, 439–449.

Julian, P. R., 1971: Some aspects of variance spectra of synoptic scale tropospheric wind components in midlatitudes and in the tropics. *Mon. Wea. Rev.*, **99**, 954–965.

Kao, S. K., and H. N. Lee, 1977: The nonlinear interactions and maintenance of the large-scale moving waves in the atmosphere. *J. Atmos. Sci.*, **34**, 471–485.

Kraichnan, R., 1967: Inertial ranges in two-dimensional turbulence. *Phys. Fluids*, **10**, 1417–1423.

Lindzen, R. S., E. S. Batten and J. W. Kim, 1968: Oscillations in atmospheres with tops. *Mon. Wea. Rev.*, **96**, 133–140.

Lau, N. C., 1979: The observed structure of tropospheric stationary waves and the local balances of vorticity and heat. *J. Atmos. Sci.*, **36**, 996–1016.

Manabe, S., D. G. Hahn and J. L. Holloway, Jr., 1974: The seasonal variation of the tropical circulation as simulated by a global model of the atmosphere. *J. Atmos. Sci.*, **31**, 43–83.

Pratt, R. W., 1976: The interpretation of space-time spectral quantities. *J. Atmos. Sci.*, **33**, 1060–1066.

——, 1977: Space-time kinetic energy spectra in mid-latitudes. *J. Atmos. Sci.*, **34**, 1054–1057.

——, 1979: A space-time spectral comparison of the NCAR and GFDL general circulation models to the atmosphere. *J. Atmos. Sci.*, **36**, 1681–1691.

——, and J. M. Wallace, 1976: Zonal propagation characteristics of large-scale fluctuations in the mid-latitude troposphere. *J. Atmos. Sci.*, **33**, 1184–1194.

Rao, M. S. V., W. V. Abbot III and J. S. Theon, 1976: Satellite derived global oceanic rainfall atlas (1973 and 1974). NASA SP-410, 186 pp.

Schäfer, J., 1979: A space-time analysis of tropospheric planetary waves in the Northern Hemisphere. *J. Atmos. Sci.*, **36**, 1117–1123.

Smagorinsky, J., 1953: The dynamical influence of large-scale heat sources and sinks on the quasi-stationary mean motions of the atmosphere. *Quart. J. Roy. Meteor. Soc.*, **79**, 342–366.